Significance of the presence of antibiotics on the a microbial consortium in wastewater - the case of nitrofurantoin and furazolidone

Agata Zdarta[1], Wojciech Smułek[1], Zuzanna Bielan[2], Jakub Zdarta[3], Luong N. Nguyen[4], Agnieszka Zgoła-Grześkowiak[5], Long D. Nghiem[4], Teofil Jesionowski[3], Ewa Kaczorek[1]*

[1] Institute of Chemical Technology and Engineering, Faculty of Chemical Technology, Poznan University of Technology, Berdychowo 4, 60-965 Poznan, Poland

[2] Department of Chemical Technology, Faculty of Chemistry, Gdansk University of Technology, G. Narutowicza 11/12, 80-233 Gdansk, Poland

[3] Faculty of Chemical Technology, Institute of Chemical Technology and Engineering, Poznan University of Technology, Berdychowo 4, 60-965 Poznan, Poland

[4] Centre for Technology in Water and Wastewater, School of Civil and Environmental Engineering, University of Technology Sydney, 81-113 Broadway, Ultimo NSW 2007, Australia

[5] Institute of Chemistry and Technical Electrochemistry Poznan University of Technology, Berdychowo 4, 60-965 Poznan, Poland

Corresponding authors: Ewa Kaczorek ewa.kaczorek@put.poznan.pl;

Highlights

- Nitrofurantoin and furazolidone had no adverse effect on the microbial consortium.
- The consortium behavior and degradation of antibiotics differed between the drugs.
- NFT reduced organic carbon consumption and increased EPS and VOC production.
- FZD decomposition exceed 60% with a small reduction of organic carbon assimilation.
- The consortium behaviour was better represented by the logistic mathematical model.

48 **Abstract**

49 Antibiotics presence in wastewater leads to migration of pollutants and disrupts natural

50 processes of mineralization of organic matter. In order to understand the mechanism of

51 this, research was undertaken on the influence of nitrofurantoin (NFT) and furazolidone

52 (FZD), on the behaviour of a consortium of microorganisms present in a model

53 wastewater in a bioreactor. Our study confirmed biodegradation of the antibiotics by the

54 microbial consortium, with the degradation efficiency within 10 days of 65% for FZD,

55 but only 20% for NFT. The kinetic study proved that the presence of analysed antibiotics

56 had no adverse effect on the microbes, but the consortium behaviour differ significantly

57 with the NFT reducing the consumption of organic carbon in wastewater and increasing

58 the production of extracellular biopolymeric and volatile organic compounds, and the

59 FZD reducing assimilation of other carbon sources to a less extent, at the expense of

60 cellular focus on biodegradation of this antibiotic.

61

62 **Keywords:** nitrofurantoin, furazolidone, kinetics, microbial consortium, wastewater

63

64 **1. Introduction**

65 At the time of growing concern about antimicrobial resistance, the antibiotic nitrofurans

66 remain their effectiveness even against antibiotic-resistant bacteria. This might be due to

67 their multiple mechanisms of action such as inhibition of DNA and RNA synthesis, a

68 metabolic enzyme, carbohydrate metabolism, and reactive oxygen species production

69 (Gallardo-Garrido et al., 2020). In 2019, the World Health Organization (WHO) listed

70 nitrofurans as important antimicrobials for human medicine (WHO, 2019). Currently,

71　nitrofurans are widely used in the treatment of urinary tract infections (Vass et al., 2008),

72　and are tested as antitubercular agents (Elsaman et al., 2019).

73　Although the administration of nitrofurans has been effective, their high elimination from

74　human and animals may raise concerns. For nitrofurantoin (NFT), 90% of the total dose

75　is eliminated in the urine, with up to 50% excreted in unchanged form in humans

76　(DrugBank Online, 2021). Similarly, 55–65% of the primary dose of furazolidone (FZD)

77　is eliminated by renal excretion in humans and animals (White, 1989). These antibiotics

78　residues can enter the wastewaters and soil, where sorption onto organic particles occurs

79　(Cycoń et al., 2019; Nguyen et al., 2019a; 2020). Recent studies revealed, that NFT

80　sorption in sediments and soils depends on the ionic strength and pH of the sorbent and

81　can range from 3.967 to 5.121 mL g^{-1}, and from 3.634 up to 43.06 mL g^{-1} in sediments

82　and soils, respectively (Tolić et al., 2019). Therefore, both nitrofuran drugs, NFT and

83　FZD, may cause serious environmental problems due to their high ecotoxicity

84　(Lewkowski et al., 2019). Mutagenicity and ecotoxicity of nitrofuran derivatives to

85　environmental organisms have been investigated since 80s. Macri' and Sbardella (1984)

86　found that the highest toxicity to *Selenastrum capricornutum* and *Daphnia magna* possess

87　nitrofurazone, followed by furaltadone tertrate and furaltadone chlorohydrate. Significant

88　toxicity of FZD on *Culex pipiens* and *Daphnia magna* was also reported later by Macrì

89　et al. (1988). More recent studies described the negative effect of furaltadone on *Ulva*

90　*lactuca* (microalgae) (Leston et al., 2011) and the significant toxicity of FZD and NFT

91　on *Aliivibrio fischeri* (bacteria) and *Heterocypris incongruens* (crustaceans) (Lewkowski

92　et al., 2019).

93　For both, environmental sorption (Tolic, et al. 2019) and biodegradation (Pacholak, et al.

94　2019) only limited studies on the process kinetics are available. However, literature

reports describing the fate of antibiotics in the environment, including municipal wastewater, focus on extremely different studies that are difficult to compare (Chaturvedi et al., 2021; Ruan et al., 2020; Wu et al., 2011). The first group consists of studies on biodegradation pathways and effects of pharmaceuticals on single and defined strains of microorganisms (e.g. Pan et al., 2018). The second group of studies includes those conducted with real wastewater and a complex consortium of microorganisms (e.g. Tang et al., 2017; Tolić et al., 2019). There are relatively few works of an indirect character, being a simplification of the real system, however verifying the phenomena on the macro level (e.g. Azimi et al., 2017; Peng et al., 2018; Miran et al., 2018). To fill in these knowledge gaps, we decided to analyse a close-to-real system based on the results of the strictly molecular and simplified systems based on our previous experience Pacholak et al. (2019). In previous study the NFT degradation was conducted and the kinetics of the process performed by single strains in simplified culture, with NFT as the only carbon source (Pacholak et al., 2019).

To mimic better the environmental conditions, and analyse the processes from a broader perspective we choose a system containing synthetic wastewater with a consortium of microorganisms of known composition, and the aim of this study was to understand the effect of the presence of NFT and FZD on the behaviour of the microorganisms. Therefore, analyses of growth kinetics, organic matter assimilation and antibiotic biodegradation were undertaken, with appropriate mathematical models proposed for the results obtained for greater precision. Nevertheless, an important aspect of the research was the analysis of the chemical composition of biomasses, as well as the profile of volatile organic compounds, as valuable markers of changes in the cell metabolism of the bacteria forming the consortium.

2. Materials and methods

2.1. Chemicals and bacterial strains

Nitrofurantoin (NFT), furazolidone (FZD), and Luria-Bertani broth (LB broth) were purchased from Sigma-Aldrich (Poland). Organic solvents and chemicals were analytical grade. Synthetic wastewater was prepared according to OECD procedure (160 mg peptone; 110 mg meat extract; 30 mg urea; 28 mg K_2HPO_4; 7 mg NaCl; 4 mg CaCl x 2 H_2O; 2 mg $MgSO_4$ x 7 H_2O) (*OEDC*, 2001).

 Five bacterial strains including, *Glutamicibacter nicotianae* AsK3a (K3a, GenBank MK503993.1), *Arthrobacter* sp. AsK4c (K3c, GenBank MN960430.1), *Ochrobactrum* sp. AsP4c (P4c, GenBank MN960431.1), *Pseudomonas aeruginosa* Asp4a (P4a, GenBank MK503653.1), and *Arthrobacter* sp. strain AsP3d (P3d, GenBank MN960429.1) were selected for the study. To obtain the bacterial consortium for this study, each strain was incubated at 25 °C for approximately 48 h until the optical density at 600 nm exceeded 1. The cultures were then centrifuged and resuspended in synthetic wastewater until an optical density of $OD_{600} \approx 1.0$ (corresponding to 1×10^8 CFU mL^{-1}). Finally, 50 mL of each suspension was mixed together (in equal volumetric proportions) to make the microbial consortium, which was used further to inoculate the batch culture.

2.2. Biodegradation experiment

The microbes were enumerated in LB broth for 24 h, centrifuged and re-dissolved in synthetic wastewater A laboratory-scale bioreactor with 1.5 L (Fig. S1 in E-supplementary data of this work, which can be found in online version of the paper) working volume was used in the experiments (Biostat B plus, Sartorius). The created bacterial consortium was cultured for 24 h in a batch reactor with 1.5 L of synthetic

143 wastewater, at 25 °C and with stirring 150 rpm to enumerate bacteria. Antibiotic, NFT or

144 FZD, was added into each bioreactor at 5 mg L^{-1} after 24 h to begin the degradation kinetic

145 experiment for another 10 days. During the period of 10 days, the operation conditions

146 were maintained at 25 °C and 150 rpm. Any potential photodegradation of antibiotics in

147 the reactor was avoided by keeping it in darkness. Sample (30 mL) was taken every day

148 for 10 days, centrifuged and stored at -20 °C for further analysis. For the control batch,

149 synthetic sludge without any additions was used.

150   *2.3. NFT and FZD concentration analysis*

151 High performance liquid chromatograph with tandem mass spectrometry detector

152 (HPLC-MS/MS) was used to determine the residual NFT and FZD content in the

153 biodegradable samples. The system consists of the UltiMate 3000 RSLC chromatograph

154 from Dionex and the API 4000 QTRAP triple quadrupole mass spectrometer from AB

155 Sciex. The samples taken during the experiment were introduced in the amount of 5 μL

156 on the Gemini-NX C18 chromatography column (100 mm × 2.0 mm i.d.; 3 μm) from

157 Phenomenex maintained at 35 °C. The mobile phase consisting of 5 mM ammonium

158 acetate in water and methanol was flowing through the column at a rate of 0.3 μL min^{-1}.

159 The gradient elution was performed by linearly increasing the percentage of organic

160 modifier from 75 to 80% in 2 min and then from 80 to 100% in 1 min. A pre-run time of

161 3 min was used before the next injection. The column eluate was directed to the

162 electrospray ionization source (the Turbo Ion Spray) of the mass spectrometer. The Turbo

163 Ion Spray source operated in positive and negative ion mode for FZD and NFT

164 respectively. The following settings were used for the ion source and mass spectrometer:

165 curtain gas 10 psi, nebulizer gas 40 psi, auxiliary gas 40 psi, temperature 400 °C, ion

166 spray voltage +/-4500 V, declustering potential +/-60 V and collision gas set to medium.

167 The dwell time for each mass transition detected in the selected reaction- monitoring

168 mode was set to 200 ms. The quantitative transition for FZD was from 226 to 122 m/z at

169 collision energy set to 29 eV and collision cell exit potential was set to 6 V. The

170 confirmatory transition was from 226 to 95 m/z at collision energy set to 21 eV and

171 collision cell exit potential was set to 4 V. The quantitative transition for NFT was from

172 237 to 152 m/z at collision energy set to -17 eV and collision cell exit potential was set

173 to -10 V. The confirmatory transition was from 237 to 124 m/z at collision energy set to

174 -20 eV and collision cell exit potential was set to -10 V.

175   *2.4. Bacterial biomass analysis*

176 The infrared (IR) spectroscopic analysis of lyophilized bacterial biomass was intended to

177 highlight specific groups on biomass surface, what allows to evaluate the biomass

178 composition changes, as well as to verify if the drugs were adsorbed on the bacteria

179 surface (what could confirm by presence of IR signals characteristic for nitrofurans). The

180 bacterial biomass was separated by centrifugation (4500 rpm, 20 min, 4 °C). The cells

181 pellet elemental composition and chemometric analysis were performed, while the liquid

182 culture was used in further experiments. The biomass was weighted and afterwards

183 lyophilized for 48 h, -50 °C, 0.36 mbar (Alpha 1.4 LD plus, Christ). Elemental analysis

184 of nitrogen, carbon, hydrogen and sulphur content in samples was performed for 7 mg

185 samples on Vario EL Cube apparatus (Elementar) to trace the dynamics of the elements

186 during decomposition process. ATR-FTIR spectroscopy was used to determine the

187 occurrence of the chemical functional groups on the surface of lyophilized cells biomass

188 (Vario 70, Bruker).

189   *2.5. Organic matter metabolism in microbial cultures*

190   *2.5.1. Organic matter assimilation*

Total organic carbon (TOC) measurements were conducted using TOC-L analyzer (Shimadzu), equipped with OCT-L 8-port autosampler (Shimadzu). The inorganic carbon was separated from the organic one by automatic acidification of the sample. Then sample was injected into the first of the two zones of the furnace (1000 °C), where was dried and burned, and in the second zone was oxidized to CO_2 in the presence of catalyst (copper (II) oxide). The carbon concentration was calculated based on the total peak value of the measured signal, after processing with the corresponding calibration curve.

2.5.2. Production of volatile organic compounds (VOCs)

The supernatant after samples centrifugation was subjected to properties and chromatography analysis. The Volatile Organic Compounds (VOC) content was evaluated to identify the main microbial VOCs (mVOCs) components during microbial bioremoval by microextraction from the headspace (HS-SPME), followed by separation of the analytes by gas chromatography and their identification by mass spectrometry (GC-MS). The 5 mL of culture were transferred to twisted glass chromatographic vials of 20 mL volume containing 1 g of sodium chloride and 1 g of citric acid each. Successively, the samples were heated for 30 min at 60 °C, and then the PEG/PDMS fiber (Merck) adsorbent was introduced into headspace of the sample, on which the analytes were adsorbed for 10 min at 60 °C. Then, desorption from the fiber was carried out at a temperature of 250 °C for 1 min. in a gas chromatograph injector (Pegasus 4D, Leco) with a BPX-5 column (28 m, 250 μm, 0.25 μm). The analysis was carried out with helium as the carrier gas (flow 1 mL min^{-1}). The device worked in the programmed temperature changes mode: 40 °C for 2 min, increase of 20 °C min^{-1} to 100 °C, then increase of 7 °C min^{-1}. up to 280 °C. The mass spectrometer was operated in the positive ion analysis mode at a voltage of the ion source of 70 V. The identification of the analytes was carried

215   out on the basis of the obtained mass spectra on the basis of the ChromaTof software

216   spectrum library (Leco Corp.). Quantification of compounds was carried out on the basis

217   of a previously prepared calibration curve, based on the correlation between the peak area

218   in the chromatogram and the standard compound concentration.

219   *2.5.3. Production of extracellular macromolecules*

220   Surface tension measurement and emulsification assay were performed to evaluate

221   changes in extracellular compounds secretion upon antibiotics exposition. The surface

222   tension of the supernatant after centrifugation was determined using tensiometer (K20,

223   Kruss,) and DuNuoy ring method. The emulsifying activity was determined as the ratio

224   of the height of the emulsified layer to the total height that was occupied by the emulsion

225   after a defined time period. Emulsion samples of 20 mL were prepared in sterile 50 mL

226   plastic laboratory tubes, combining equal volumes of supernatant after cenrifugationand

227   hexadecane (analytical grade, Sigma-Aldrich). The samples were first mixed (Vortex 3,

228   IKA) at 2500 rpm for 15 s, and then homogenized (sonicator Sonoplus, Bandelin) in the

229   following conditions: 10 min, in cycles action/break 10 s/10 s, amplitude 16%, and cooled

230   with tap water. The emulsion stability tests were conducted after 24 h and the

231   emulsification index (E24) was calculated.

232   *2.6. Kinetic calculations*

233   To describe the kinetics of biological processes different mathematical model are

234   commonly applied. A study by Schmidt et al. (1985) contains a wide spectrum of

235   equations and discuss two main parameters of the bioprocess, i.e. biomass growth and

236   substrate concentration. They distinguished four classes of biomass growth models and

237   three options of substrate concentration. In our study, the biomass growth was observed

238   what allowed to exclude the non-growth models, that were frequently characteristic for

239   biodegradation of pharmaceuticals, what was underlined by Pan et al. (2018) in their

240   publication. As a consequence Michaelis-Menten or Monod equations cannot be applied

241   (Briones et al., 2018). Finally, after analysis of several models, the logistic growth model

242   was found as the most suitable, and it was described with the following equations in

243   standard (Eq. 1) and general differential form (Eq. 2):

244    $X(t) = \dfrac{X_{max}}{1+e^{-kt}}$ (Eq.1)

245    $\mu = \dfrac{d}{dt}X(t) = \dfrac{X_{max}ke^{-kt}}{(e^{-kt}+1)^2}$ (Eq.2)

246   where:

247   X represents the biomass concentration during the process (mg L^{-1}),

248   X_{max} represents the final biomass concentration (theoretical) (mg L^{-1}),

249   t represents the time of the process (day),

250   k represents the logistic growth rate coefficient [(mg L^{-1})$^{-1}$ day^{-1}],

251   μ represents the growth rate (mg L^{-1} day^{-1}).

252   Moreover, the kinetic curves of the function $\mu(t)$ allow calculating the maximum value of

253   the function, i.e. maximum growth rate, μ_{max}. In that case t_{max} representative the time,

254   when μ_{max} occurred. Additionally, we calculated the average growth rate, μ_{avr} as the ratio

255   of total biomass increase to the time of the process.

256   To evaluate the substrate biodegradation kinetic, first order, second order and Michaelis-

257   Menten models were considered (Jia et al., 2017; Schmidt et al., 1985). To describe the

258   relationship between the substrate concentration, mathematical models taking into

259   account polynomial equations of higher orders were also considered.

260   *2.7. Statistical analysis*

261 All the analysis were made in triplicate. The statistical significance of data was analyzed

262 using a one-way analysis of variance (ANOVA) (SigmaPlot 11.0 program). A probability

263 (P) value of <0.05 was considered significant. The data are presented as mean ± standard

264 deviation (SD).

265

266

267

3. Results and disscussion

3.1. Antibiotics degradation in bioreactor

270 Concentration measurements of the antibiotics in bioreactor cultures showed that the

271 removal of both antibiotics occurred, however, the efficiency of the antibiotics' decay

272 was different (Fig. 1A). In the first 24 h, the removal of FZD was above 50%. In the next

273 9 days, the removal increased to a maximum of 65%. On contrary, the removal of NFT

274 was 23% after 10 days experiment, with the same initial concentration of drugs equal to

275 5 mg L^{-1} (Fig. 1B). The results collected indicated that the biodegradation kinetics was in

276 the form of a third-degree equation and, especially for cultures with FZD, three stages are

277 observed - the first and the last of the accelerated substrate uptake and the middle one

278 with a significant slowdown in degradation. Table 1 presents the conclusions of the

279 polynomial (third-order) mathematical model, which showed the best fit to the

280 measurement points. It can be seen from Table 1, that the final degradation rate (on the

281 10th day) of FZD was still at the level of 0.45 mg L^{-1} and for NFT decreased down almost

282 to 0 mg L^{-1} (Fig. 1C), whereas the average substrate degradation rate (S_{avr}) calculated

283 based on the polynomial equation was significantly lower for NFT and reached 0.12 mg

284 L^{-1} day^{-1} (Table 1). The maximum biodegradation (S_{max}) of this compound occurred on

285 day 1 and was equal to 0.25 mg L^{-1} day^{-1}based on the model applied. On the contrary, the

286 FZD reached the maximum of biodegradation on day 8 with the S_{max} of 1.9 mg L^{-1} day^{-}

287 [1] and S_{avr} 0.39 mg L^{-1} day^{-1}, which confirms that the cooperation of the strains in a

288 consortium led to the higher biodegradation efficiency of this antibiotic. Nguyen et al.

289 (2019b) stated that tiamulin antibiotic was biodegraded by the bacterial consortium

290 (containing *Achromobacter*, *Delftia*, *Flavobacterium*, *Pseudomonas*, and

291 *Stenotrophomonas* strains) according to logistic model, similarly as we observed in our

292 study. However, an example of biodegradation following the first-order equation model

293 was described by Li and Zhang (2010) for cefalexin, sulfamethoxazole, sulfadiazine, and

294 three fluoroquinolones: norfloxacin, ofloxacin, and ciprofloxacin, which were degraded

295 by wastewater microorganisms.

296   *3.2. Organic matter balance*

297 Measurements of changes in total organic matter concentration shed additional light on

298 the results obtained and the kinetic study of the results was performed to evaluate biomass

299 growth parameters, changes in total organic carbon (TOC) in the samples, as well as to

300 fit the degradation curves to the existing models. At first, the biomass growth was

301 evaluated for all, cultures with antibiotics and the reference culture (control). For all tested

302 systems, it was observed that it corresponds to the logistic growth model, which was

303 confirmed by the comparison of various mathematical models to measurement points.

304 Both the graphs (Fig. 2A-D) and the kinetic parameters presented in Table 2 show that

305 the presence of antibiotics significantly influences the growth of microorganisms. What

306 is interesting, the presence of xenobiotics stimulated biomass growth (Fig. 2A). The

307 biomass growth rate profiles for batches differ significantly, indicating that the dynamics

308 of growth were the lowest for control samples (Fig. 2B-D). While in the control sample

309 the average biomass growth rate (μ_{avr}) was 4.1 mg L^{-1} day^{-1}, in the cultures with NFT and

310 FZD it was 11.0 mg L^{-1} day^{-1} and 8.4 mg L^{-1} day^{-1}, respectively (Table 2). At the same

time, the maximum growth rate (μ_{max}) was the highest in the control culture and was equal to 80 mg L^{-1} day^{-1}, which was at least twice as high as those found for the other two cultures. This suggests that in the presence of antibiotics, growth was more even, rather than abrupt, as in the control sample. Additionally, the stage of the most intensive growth (t_{max}) shortens from 6.0 days for the control culture to 2.8 days and 4.8 days in cultures with NFT and FZD, respectively (Table 2). That is an interesting outcome taking into account their multiactivity. For most of the antibiotics, the growth of the biomass is rather suspended, than improved, as was presented e. g. by Kim et al. (2020) who found that another antibiotic, ciprofloxacin in the concentration of 500 µg L^{-1} reduced by more than tenfold the relative abundance of *Rhodobacteraceae* and *Nakamurellaceae* in the analyzed samples. In another study, it has been confirmed that multi-hierarchical antibiotic selection creates an imbalance in the microbiota composition, that is hard to restore even several months after treatment (Martínez, 2017). However, the maximum biomass concentration (X_{max}), which can be calculated theoretically, was relatively similar in all cases, ranging from 303 to 348 mg L^{-1}, and was nearly the same for both cultures with the analyzed antibiotics (Table 2).

3.3. Analysis of mass transfer in biodegradation process

Analysis of the results discussed above may lead to interesting conclusions. The tested antibiotics were degraded by a consortium of microorganisms, although the reduction in NFT was relatively small. At the same time, a more significant increase in biomass was observed in the presence of these compounds than in the control sample. However, in the case of this parameter, a greater increase was observed in cultures with NFT. Moreover, both antibiotics caused significantly lower assimilation of dissolved organic matter,

which can be seen by observing changes in TOC. Based on these observations, the following course of bioreactor processes can be proposed.

- In the presence of NFT, microbial cells manifest response to stress conditions, which includes a decrease in metabolism, and a relative increase in biomass might not necessarily mean an increase in cell number, but the production of protective extracellular macromolecular compounds that coat the cells from the outside (Mathivanan et al., 2021).

- In contrast, the response to FZD is different, despite the high similarity in chemical structure between NFT and FZD. Cells focus on biodegrading FZDs instead of assimilating the remaining dissolved carbon source present in wastewater. Assimilation of FZD (and partially other organic compounds) allows for an increase in biomass, but presumably a lot of energy is used to switch the metabolic apparatus to degrading the antibiotic rather than the organic matter present in the synthetic effluent (Zavala et al., 2019).

These results show the complex competition that can exist between metabolizing a relatively readily available carbon, present for example in peptone, and a rather complex antibiotic molecule. Moreover, Liu et al., (2017) reported the importance of media concentration in degradation processes, showing that 1/5 dilution of BEP medium allowed the most efficient degradation of gentamicin. However, it is important to note that our study used strains isolated from wastewater through selective cultures supplemented with nitrofuran derivatives (Pacholak et al., 2019). This may explain the relative ease of adaptation to degrade these compounds.

3.4. Antibiotics impact on bacteria outer surface

357   According to the FTIR results, the tested compounds did not reveal a significant impact

358   on the bacterial surface (Fig. S2A in E-supplementary data of this work, which can be

359   found in online version of the paper). The infrared spectra of the untreated biomass show

360   signals at 3286 cm^{-1} (stretching vibrations of amine groups), 2932 cm^{-1} (stretching

361   vibrations of –CH, –CH$_2$ and –CH$_3$), 1075 cm^{-1} (stretching vibrations of C–O bonds) and

362   526 cm^{-1} (bending vibrations of C–C bonds). Further, peaks with maxima at 1642, 1535

363   and 1240 cm^{-1}, are characteristic for vibrations of amide I (mainly C=O stretching), amide

364   II (mainly C–N–H bending) and amide III (mainly C–N=O bending), and confirm the

365   presence of the surface functional proteins. Bacteria cultured with NFT and FZD did not

366   change significantly in comparison to untreated biomass. Moreover, comparing the

367   results to the spectra of pure NFT and FZD (Fig. S2B and S2C in E-supplementary data

368   of this work, which can be found in online version of the paper), characteristic peaks are

369   not observed in the biomass samples. By contrast, previous research reporting NFT or

370   FZD attachment to different materials confirmed effective linkage of antibiotics by the

371   presence of characteristic peaks identified on the FTIR spectra of the samples after the

372   process. Teoh et al. (2019) observed the presence of N–O, C–O and C–N stretching

373   vibrations, along with the fingerprint region of 2,5-disubstituted furan ring on co-crystal

374   NFT/citric acid spectra. Gurav et al. (2020) noted shifts of C=C and C–O bands due to

375   the interaction with N–O group from FZD. These changes were not observed for biomass

376   analysed in this study, confirming that the drugs were removed rather by degradation,

377   than sorption. This is also consistent with Zhang et al. (2013) who found almost none

378   FZD in the bacterial cells lysates after growth in FZD-containing media, proving that this

379   compound was also not accumulated inside the cells.

380 Moreover, the performed elemental analysis indicated a significant increase in nitrate and

381 carbon content in the cells biomass after cultivation with NFT or FZD. The elevated levels

382 of nitrogen and carbon, to 11.70% and 57.06% for NFT, and 10.95% and 56.51% for

383 FZD, respectively (Table S1) might be associated with bacterial growth and biomass

384 increase (Li et al., 2021). What is interesting, in all analysed experiments the C:N ratio

385 was comparable and reached the value around 5:2. This is also consistent with the biomass

386 growth kinetic measurements, where the maximum biomass concentration after 10 days

387 of experiments was ranging from 303 to 348 (mg L^{-1}) (Table 2). The impact of growth

388 conditions on bacterial C, N and P content was investigated, among others by Vrede et

389 al. (2002). They found that C limitation resulted in the lowest C:N ratio and the elemental

390 composition of the biomass changed substantially among isolates and under different

391 growth conditions (Vrede et al., 2002). This was not observed for NFT and FZD growth

392 bacterial consortia, suggesting that these substances did not act as limiting factors on

393 bacterial growth. Furthermore, measurements of total organic carbon in the samples

394 revealed doubling of the amount of the organic carbon in the samples with the TOC of

395 28.35 and 27.73 mg L^{-1} for NFT and FZD, respectively, comparing to 15.85 mg L^{-1} for

396 the control (Table S1).

397 *3.5. Changes in microbial VOCs profile*

398 The degradation of complex molecules may result in the formation of microbial volatile

399 organic compounds (mVOC), a small molecule compounds formed in every living cell.

400 However, their production is mainly the result of basic metabolism processes. The

401 emission rates and profiles of mVOCs secretion are dependable on many factors such as

402 taxonomic relationship, time of growth, temperature and type of substrate, forming

403 characteristic for the strain and compound fingerprint of the mVOCs (Insam and Seewald,

404 2010). Intense metabolism under simultaneously unfavorable conditions (e.g., lack of

405 adequate oxygen concentration as an electron acceptor) can lead to their increased

406 production when the cell does not fully mineralize carbon sources (Hidalgo et al., 2019),

407 what we observed in presented study, which documents the differences in profiles of

408 emission of mVOCs during growth on media containing NFT or FZD. To distinguish

409 mVOCs originating from NFT and FZD degradation processes the collected results were

410 compared to control samples, where synthetic wastewater was used as a sole carbon and

411 energy source. Analyses revealed the presence of the methyl ketones, alcohols, esters,

412 carboxylic acids and sulfur-containing compounds in mVOC profiles of the tested

413 cultures (Fig. 3). Moreover, distinct mVOC profiles were observed for cultures grown

414 with NFT and FZD. Although the compounds found in the samples were mostly the same,

415 the amount of mVOC created by NFT and FZD samples, as well as the proportions of

416 particular composites differs significantly (Fig. 3A). The most abundant was 1-

417 Hexanol,2-ethyl- which proportion in treated samples increased to over 70% in the

418 mVOC profile of the samples (Fig. 3B). Also, the presence in the samples of 2-Heptanone

419 raised, from 0.47% (control) to 4.03% and 9.97% for NFT and FZD, respectively which

420 was followed by a decrease in dimethyl trisulfide (DMTS) content in the samples.

421 Interestingly, only three compounds were differentiating between NFT and FZD samples

422 (5-Methyl-2-hexanone; Nonanal, and 2-Butyltetrahydro-furan). In all three cases,

423 NFT-grown cells reduced the amount of these compounds in their mVOC profile, while

424 FZD-grown cells increased their content in the mVOC profile (Fig. 3B). According to

425 Stahl and Parkin (1996), microbial production of volatile organic compounds of bacteria

426 treated with streptomycin varied significantly in respect of the total amount of VOC and

427 their profile in different periods. The authors observed increased production of mVOCs

428   in samples treated with the antibiotic, comparing to other treatment (Stahl and Parkin,

429   1996), which is consistent with our results. Presented in our study mVOCs were also

430   detected in decomposition soil samples by Perrault et al. (2014). Compounds reported as

431   the most abundant in our research, mainly ketones and alcohols are a common result of

432   macromolecules breakdown. Interestingly, compound abundant in higher concentration

433   in FZD samples (where the degradation was more pronounced) were detected only in

434   decomposition soil samples during active decay of carrion (Nonanol and 2-

435   Butyltetrahydro-furan) or in dry remains (5-Methyl-2-hexanone). 1-Hexanol,2-ethyl- was

436   identified only during the fresh tissue breakdown, while 2-Heptanone was present during

437   active and advanced decay, as well as in dry remains (Perrault et al., 2015). Moreover,

438   the authors point out that sulphur-containing compounds, like DMTS in our study, are

439   one of the most abundant compounds in decomposition profiles. They might originate

440   from the degradation of sulphur-containing amino acids or metabolic processes during

441   anaerobic decomposition. It is also worth notice, that the mVOCs analysis undertaken in

442   our study did not detect the presence of aniline and 2-fluoroaniline, the volatile markers

443   of nitroreductase activity in the wide range of cells (Thompson et al., 2020).

444   *3.6. Extracellular compounds production*

445   Moreover, the performed analysis of surface tension of the cell culture supernatant and

446   emulsification analysis revealed some modifications which may lead to increased

447   bioavailability of low-soluble drugs molecules. The surface tension of the liquid culture

448   after 10 days decreased slightly, from 65.02 (control) to 61.84 mN m^{-1} and 62.22 mN m^{-1}

449   for NFT and FZD, respectively (Table S1). Furthermore, the emulsification indexes

450   (EI24) of the cultures grown on NFT and FZD have increased in comparison to control

451   cells, reaching the highest value of 7.82% when NFT was added to the batch. The decline

452 in surface tension and increase in emulsifying properties of bacterial cultures is usually

453 associated with the production of some surface-active molecules. In this case, the

454 observed slight changes in surface tension and an increase in emulsification index value

455 indicates that the molecules excreted by the cells are rather bioemulsifieres, e.g.

456 exopolysaccharide (EPS), than biosurfactants. Thanks to the high number of reactive

457 groups on the EPS surface they stabilize the emulsion, which increases the solubility of

458 poorly-soluble substrates and increase their bioavailability (Uzoigwe et al., 2015).

459

460 **4. Conclusions**

461 The presented study thoroughly examined the bioremoval of NFT and FZD by the

462 microbial consortium in wastewater model system. The two antibiotics affected

463 consortium behaviour and overall organic matter metabolism in very different ways. The

464 differences in degradation efficiency highlighted the importance of primary and

465 alternative carbon sources, and the behaviour of a mix of the microorganisms can be better

466 represented by the logistic mathematical model. Moreover, the overproduction of

467 mVOCs, especially 2-ethylhexan-1-ol in the analyzed cases, might be an important

468 marker of stress conditions. This study is a valuable contribution to the current knowledge

469 on biodegradation of nitrofuran derivatives.

470

471 **Acknowledgements**

474 **Funding**

CRediT authorship contribution statement

Agata Zdarta: Conceptualization, Data curation, Formal analysis, Investigation, Visualization, Writing – original draft; **Wojciech Smułek**: Conceptualization, Data curation, Formal analysis, Investigation, Methodology, Visualization, Writing – original draft; **Zuzanna Bielan**: Formal analysis, Investigation, Visualization; **Jakub Zdarta**: Data curation, Formal analysis, Investigation, Writing – original draft; **Luong N. Nguyen**: Investigation, Visualization, Writing – original draft; **Agnieszka Zgoła-Grześkowiak**: Formal analysis, Methodology; **Long D. Nghiem**: Conceptualization, Supervision, Writing - review & editing; **Teofil Jesionowski**: Project administration, Supervision, Writing - review & editing; **Ewa Kaczorek**: Conceptualization, Funding acquisition, Project administration, Resources, ; Supervision, Writing - review & editing

Declaration of Competing Interest

The authors declare that they have no known competing financial interests or personal relationships that could have appeared to influence the work reported in this paper.

References

1. Azimi, N., Najafpour, G.D., Hassani, A.H., Borghei S.M., 2018. Simultaneous sulfamethoxazole and trimethoprim removal and biofilm growth characteristics in attached growth bioreactor. Int. J. Environ. Sci. Technol. 15, 415–426.

2. Briones, R.M., Zhuang, W.Q., Sarmah, A.K., 2018. Biodegradation of metformin and guanylurea by aerobic cultures enriched from sludge. Environ. Pollut. 243, 255–262.

3. Chaturvedi, P., Giri, B.S., Shukla, P., Gupta, P., 2021. Recent advancement in

499   remediation of synthetic organic antibiotics from environmental matrices:

500   Challenges and perspective. Bioresour. Technol. 319, 124161.

501   4. Cycoń, M., Mrozik, A., Piotrowska-Seget, Z., 2019. Antibiotics in the soil

502   environment—degradation and their impact on microbial activity and diversity.

503   Front. Microbiol. 10, 338.

504   5. DrugBank Online, 2021. Nitrofurantoin [WWW Document]. DrugBank Online.

505   URL https://go.drugbank.com/drugs/DB00698 (accessed 1.16.21).

506   6. Elsaman, T., Mohamed, M.S., Mohamed, M.A., 2019. Current development of 5-

507   nitrofuran-2-yl derivatives as antitubercular agents. Bioorg. Chem. 88, 102969.

508   7. Gallardo-Garrido, C., Cho, Y., Cortés-Rios, J., Vasquez, D., Pessoa-Mahana,

509   C.D., Araya-Maturana, R., Pessoa-Mahana, H., Faundez, M., 2020. Nitrofuran

510   drugs beyond redox cycling: Evidence of Nitroreduction-independent cytotoxicity

511   mechanism. Toxicol. Appl. Pharmacol. 401, 115104.

512   8. Guay, D.R., 2001. An update on the role of nitrofurans in the management of

513   urinary tract infections. Drugs 61, 353–364.

514   9. Gurav, R., Bhatia, S.K., Choi, T.R., Park, Y.L., Park, J.Y., Han, Y.H., Vyavahare,

515   G., Jadhav, J., Song, H.S., Yang, P., Yoon, J.J., Bhatnagar, A., Choi, Y.K., Yang,

516   Y.H., 2020. Treatment of furazolidone contaminated water using banana

517   pseudostem biochar engineered with facile synthesized magnetic

518   nanocomposites. Bioresour. Technol. 297, 122472.

519 10. Hidalgo, K., Ratel, J., Mercier, F., Gauriat, B., Bouchard, P., Engel, E., 2019.

520   Volatolomics in bacterial ecotoxicology, a novel method for detecting signatures

521   of pesticide exposure? Front. Microbiol. 9, 3113.

522 11. Insam, H., Seewald, M.S.A., 2010. Volatile organic compounds (VOCs) in soils.

523   Biol. Fertil. Soils 46, 199–213.

524 12. Jia, Y., Khanal, S.K., Zhang, H., Chen, G.H., Lu, H., 2017. Sulfamethoxazole

525   degradation in anaerobic sulfate-reducing bacteria sludge system. Water Res. 119,

526   12–20.

527 13. Kim, D., Nguyen, L.N., Oh, S., 2020. Ecological impact of the antibiotic

528   ciprofloxacin on microbial community of aerobic activated sludge. Environ.

529   Geochem. Health 42, 1531–1541.

530 14. Leston, S., Nunes, M., Viegas, I., Lemos, M.F.L., Freitas, A., Barbosa, J., Ramos,

531   F., Pardal, M.A., 2011. The effects of the nitrofuran furaltadone on Ulva lactuca.

532   Chemosphere 82, 1010–1016.

533 15. Lewkowski, J., Rogacz, D., Rychter, P., 2019. Hazardous ecotoxicological impact

534   of two commonly used nitrofuran-derived antibacterial drugs: Furazolidone and

535   nitrofurantoin. Chemosphere 222, 381–390.

536 16. Li, B., Zhang, T., 2010. Biodegradation and adsorption of antibiotics in the

537   activated sludge process. Environ. Sci. Technol. 44, 3468–3473.

538 17. Li, W., Shi, C., Yu, Y., Ruan, Y., Kong, D., Lv, X., Xu, P., Awasthi, M.K., Dong,

539   M., 2021. Interrelationships between tetracyclines and nitrogen cycling processes

540   mediated by microorganisms: A review. Bioresour. Technol. 319, 124036.

541 18. Liu, Y., Chang, H., Li, Z., Feng, Y., Cheng, D., Xue, J., 2017. Biodegradation of

542   gentamicin by bacterial consortia AMQD4 in synthetic medium and raw

543   gentamicin sewage. Sci. Rep. 7, 1–11.

544 19. Macri', A., Sbardella, E., 1984. Toxicological evaluation of nitrofurazone and

545   furaltadone on Selenastrum capricornutum, Daphnia magna, and Musca

546   domestica. Ecotoxicol. Environ. Saf. 8, 101–105.

547   20. Macrì, A., Stazi, A. V., Dojmi Di Delupis, G., 1988. Acute toxicity of furazolidone on Artemia salina, Daphnia magna, and Culex pipiens molestus larvae. Ecotoxicol. Environ. Saf. 16, 90–94.

550   21. Martínez, J.L., 2017. Effect of antibiotics on bacterial populations: A multi-hierachical selection process. F1000Research 6, 51.

552   22. Mathivanan, K., Chandirika, J.U., Mathimani, T., Rajaram, R., Annadurai, G., Yin, H., 2021. Production and functionality of exopolysaccharides in bacteria exposed to a toxic metal environment. Ecotoxicol. Environ. Saf. 208, 111567.

555   23. Miran, W., Jang, J., Nawaz, M., Shahzad, A., Lee, D.S., 2018. Biodegradation of the sulfonamide antibiotic sulfamethoxazole by sulfamethoxazole acclimatized cultures in microbial fuel cells. Sci. Total Environ. 627, 1058–1065.

558   24. Mohammad, N.S., Safian, M.F., Ariffin, S.H.Z., Ariffin, Z.Z., 2018. Biortansformation of nitrofurans antibiotics by Aspergillus species - residual antibacterial activity. Malaysian J. Biochem. Mol. Biol. 2, 28–33.

561   25. Nguyen, L.N., Commault, A.S., Sutherland, D., Semblante, G.U., Oh, S., Nghiem, L.D., 2020. Contemporary methods for removal of nonsteroidal anti-inflammatory drugs in water reclamations, in.Barceló, D., Kostianoy, A.G. (Eds.), Handbook of Environmental Chemistry. Springer Science and Business Media Deutschland GmbH, pp. 217–239.

566   26. Nguyen, L.N., Nghiem, L.D., Pramanik, B.K., Oh, S., 2019. Cometabolic biotransformation and impacts of the anti-inflammatory drug diclofenac on activated sludge microbial communities. Sci. Total Environ. 657, 739–745.

569   27. Nguyen, X.T.K., Pinyakong, O., Thayanukul, P., 2019. Bacterial community structures and biodegradation kinetic of Tiamulin antibiotic degrading enriched

571   consortia from swine wastewater. J. Environ. Heal. Sci. Eng. 17, 1121–1130.

572   28. Pacholak, A., Smułek, W., Zgoła-Grześkowiak, A., Kaczorek, E., 2019.

573   Nitrofurantoin—microbial degradation and interactions with environmental

574   bacterial strains. Int. J. Environ. Res. Public Health 16, 1526.

575   29. Pan, L.J., Li, J., Li, C.X., Tang, X. Da, Yu, G.W., Wang, Y., 2018. Study of

576   ciprofloxacin biodegradation by a Thermus sp. isolated from pharmaceutical

577   sludge. J. Hazard. Mater. 343, 59–67.

578   30. Peng, P., Huang, H., Ren, H., 2018. Effect of adding low-concentration of

579   rhamnolipid on reactor performances and microbial community evolution in

580   MBBRs for low C/N ratio and antibiotic wastewater treatment. Biores. Technol.

581   256, 557–561.

582   31. Perrault, K.A., Rai, T., Stuart, B.H., Forbes, S.L., 2015. Seasonal comparison of

583   carrion volatiles in decomposition soil using comprehensive two-dimensional gas

584   chromatography-time of flight mass spectrometry. Anal. Methods 7, 690–698.

585   32. Plakas, S.M., El Said, K.R., Stehly, G.R., 1994. Furazolidone disposition after

586   intravascular and oral dosing in the channel catfish. Xenobiotica 24, 1095–1105.

587   33. Ruan, Y., Kumar Awasthi, M., Cai, L., Lu, H., Xu, X., Li, W., 2020. Simultaneous

588   aerobic denitrification and antibiotics degradation by strain Marinobacter

589   hydrocarbonoclasticus RAD-2. Bioresour. Technol. 313, 123609.

590   34. Schmidt, S.K., Simkins, S., Alexander, M., 1985. Models for the kinetics of

591   biodegradation of organic compounds not supporting growth. Appl. Environ.

592   Microbiol. 50, 323–331.

593   35. Stahl, P.D., Parkin, T.B., 1996. Microbial production of volatile organic

594   compounds in soil microcosms. Soil Sci. Soc. Am. J. 60, 821–828.

595   36. Tang, K., Escola Casas, M., Ooi, G.T.H., Kaarsholm, K.M.S., Bester, K.,

596   Andersen, H.R., 2017. Influence of humic acid addition on the degradation of

597   pharmaceuticals by biofilms in effluent wastewater. Int. J. Hyg. Environ. Health

598   220, 604–610.

599   37. Test No. 303: Simulation Test - Aerobic Sewage Treatment -- A: Activated

600   Sludge Units; B: Biofilms, 2001. , OECD Guidelines for the Testing of Chemicals,

601   Section 3. OECD.

602   38. Thompson, R., Perry, J.D., Stanforth, S.P., Dean, J.R., 2020. Detection of

603   microbial nitroreductase activity by monitoring exogenous volatile organic

604   compound production using HS-SPME-GC-MS. Separations 7, 64.

605   39. Tolić, K., Mutavdžić Pavlović, D., Židanić, D., Runje, M., 2019. Nitrofurantoin

606   in sediments and soils: Sorption, isotherms and kinetics. Sci. Total Environ. 681,

607   9–17.

608   40. Uzoigwe, C., Burgess, J.G., Ennis, C.J., Rahman, P.K.S.M., 2015. Bioemulsifiers

609   are not biosurfactants and require different screening approaches. Front.

610   Microbiol. 6, 245.

611   41. Vass, M., Hruska, K., Franek, M., 2008. Nitrofuran antibiotics: a review on the

612   application, prohibition and residual analysis. Vet. Med. (Praha). 53, 469–500.

613   42. Vrede, K., Heldal, M., Norland, S., Bratbak, G., 2002. Elemental composition (C,

614   N, P) and cell volume of exponentially growing and nutrient-limited

615   bacterioplankton. Appl. Environ. Microbiol. 68, 2965–2971.

616   43. White, A.H., 1989. Absorption, distribution, metabolism, and excretion of

617   furazolidone: A review of the literature. Scand. J. Gastroenterol. 24, 4–10.

618   44. WHO, 2019. Critically important antimicrobials for human medicine, WHO.

619   World Health Organization.

620   45. Wu, X., Wei, Y., Zheng, J., Zhao, X., Zhong, W., 2011. The behavior of

621   tetracyclines and their degradation products during swine manure composting.

622   Bioresour. Technol. 102, 5924–5931.

623   46. Zavala, N., Baeza, L., Gonzalez, S., Choudhary, M., 2019. The effects of different

624   carbon sources on the growth of Rhodobacter sphaeroides. Adv. Microbiol. 9,

625   737–749.

626   47. Zhang, W., Niu, Z., Yin, K., Liu, F., Chen, L., 2013. Degradation of furazolidone

627   by bacteria Acinetobacter calcoaceticus T32, Pseudomonas putida SP1 and

628   Proteus mirabilis V7. Int. Biodeterior. Biodegrad. 77, 45–50.

629

Figure captions

Fig. 1. Nitrofurantoin (NFT) and furazolidone (FZD): (A) Biological removal rates; (B) changes of drugs concentration, and (C) daily degradation rate during 10-days experiment. Samples markers: NFT supplemented (♦), and FZD supplemented (●) batches.

Fig. 2. Changes in: (A) biomass concentration and (E) TOC concentration of the tested systems; (B-D) kinetic study of biomass growth rate changes and (F-H) relative TOC concentration changes; samples markers: control (▲), NFT supplemented (♦), and FZD supplemented (●) batches.

Fig. 3. Liquid culture volatile organic compounds (A) proportions, and (B) relative VOCs content after 10 days experiment;
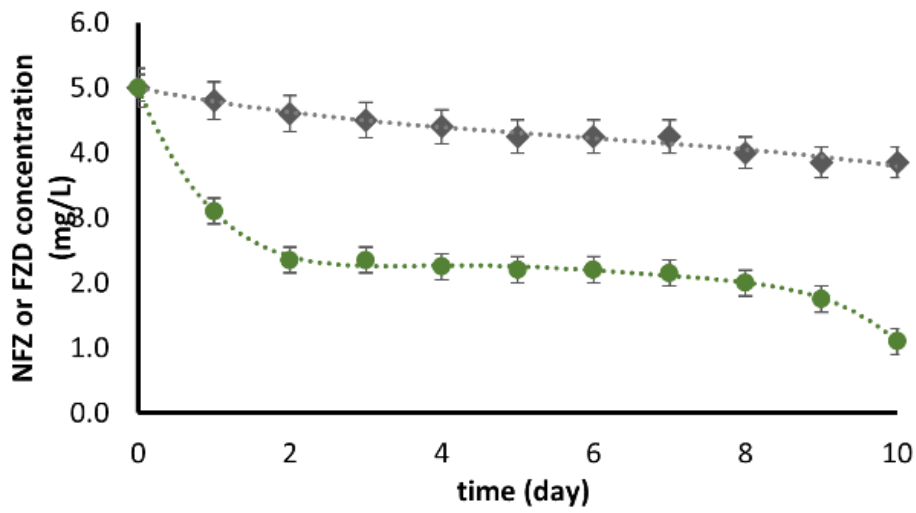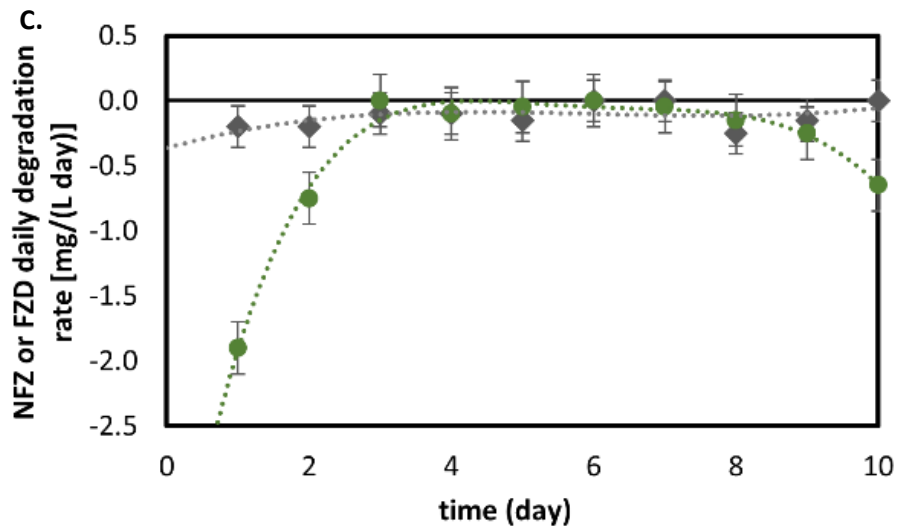
649   **Fig. 1**

A.

650

B.

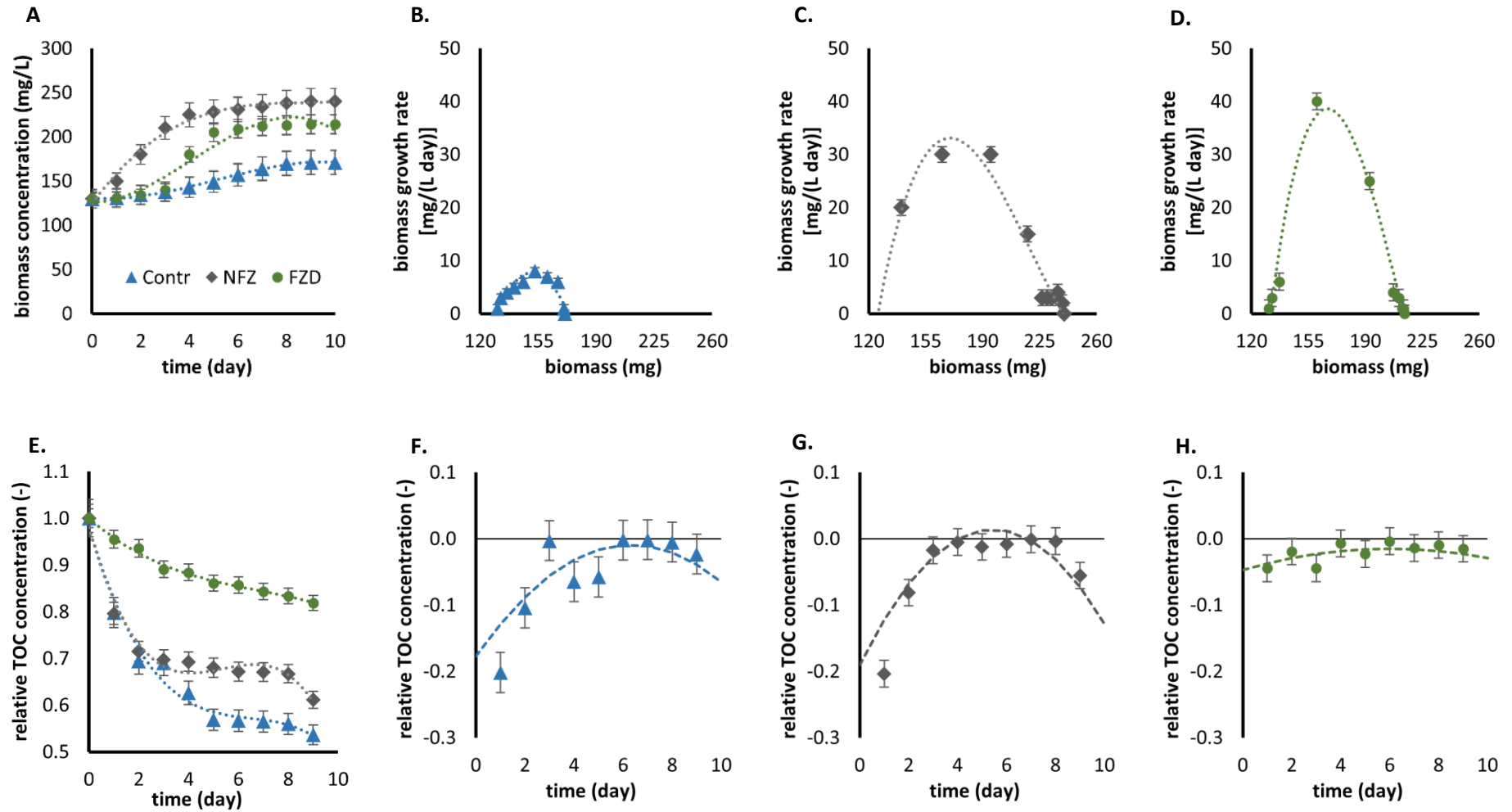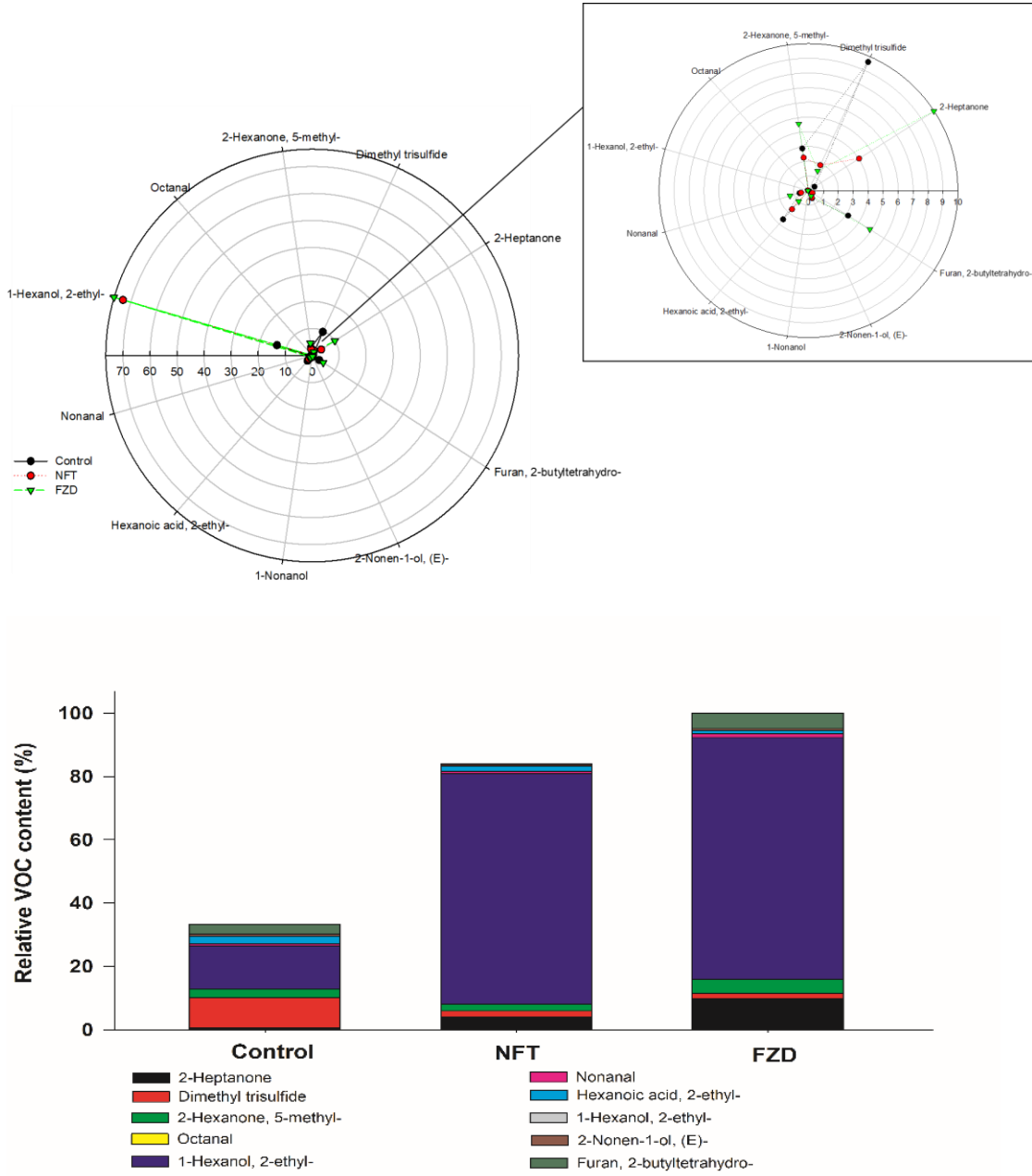651   C.
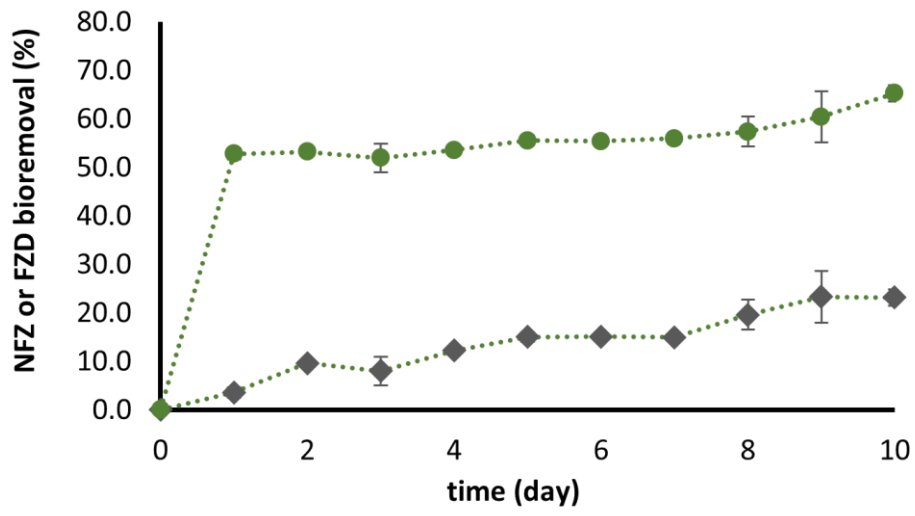
652

653   **Fig. 2**

654

655   **Fig. 3**

658

659 **Table 1. Substrate biodegradation models parameters**

Parameter	NFT	FZD
S_{avr} (mg L^{-1} day^{-1})	0.12	0.39
S_{max} (mg L^{-1} day^{-1})	0.25	1.90
t_{max} (day)	1	8

660 **S_{avr}** – average substrate degradation rate; **S_{max}** – maximum substrate degradation rate;

661 **t_{max}** – the day of maximum substrate degradation rate

662

663   **Table 2. Biomass growth parameters**

	Control	NFT	FZD
k [(mg L^{-1})$^{-1}$ day^{-1}]	4.31	2.66	7.87
X$_{max}$ (mg L^{-1})	303	348	342
μ$_{max}$ (mg L^{-1} day^{-1})	80	30	40
t$_{max}$ (day)	6.0	2.8	4.8
μ$_{avr}$ (mg L^{-1} day^{-1})	4.1	11.0	8.4
μ$_{max}$/ μ$_{avr}$ (-)	19.5	2.7	4.8

664   **k** – the logistic growth rate coefficient; **X$_{max}$** – the maximum biomass concentration; **μ$_{max}$**

665   – the maximum growth rate; **t$_{max}$** – the day of maximum biomass growth rate; **μ$_{avr}$** – the

666   average biomass growth rate; **μ$_{max}$ / μ$_{avr}$** – the maximum growth rate/ the average biomass

667   growth rate ratio